PHYSICAL REVIEW MATERIALS **5**, 114404 (2021)

Stable polar oxynitrides through epitaxial strain

Li Zhu,[1,*] Hiroyuki Takenaka,[1,2] and R. E. Cohen[1,†]
[1]*Extreme Materials Initiative, Earth and Planets Laboratory, Carnegie Institution for Science,*
5241 Broad Branch Road, NW, Washington, DC 20015, USA
[2]*Department of Chemistry and Biochemistry, University of California, Santa Cruz, California 95060, USA*

(Received 14 August 2020; revised 1 June 2021; accepted 26 October 2021; published 15 November 2021)

We investigate energetically favorable structures of ABO_2N oxynitrides as functions of pressure and strain via swarm-intelligence-based structure prediction methods, density functional theory (DFT) lattice dynamics and first-principles molecular dynamics. We predict several thermodynamically stable polar oxynitride perovskites under high pressures. In addition, we find that ferroelectric polar phases of perovskite-structured oxynitrides can be thermodynamically stable and synthesized at high pressure on appropriate substrates. The dynamical stability of the ferroelectric oxynitrides under epitaxial strain at ambient pressure also implies the possibility to synthesize them using pulsed laser deposition or other atomic layer deposition methods. Our results have broad implications for further exploration of other oxynitride materials as well. We performed first-principles molecular dynamics and find that the polar perovskite of $YSiO_2N$ ($I4cm$) is metastable up to at least 600 K under compressive epitaxial strain before converting to the stable wollastonitelike structures ($I4/mcm$). We predict that $YGeO_2N$, $LaSiO_2N$, and $LaGeO_2N$ are metastable as ferroelectric perovskites ($P4mm$) at zero pressure even without epitaxial strain.

DOI: 10.1103/PhysRevMaterials.5.114404

The perovskite oxides (ABO_3) form one of the most widely studied groups in condensed matter physics and materials science. Extensive studies over decades show that perovskite oxides possess an exceptional diversity of physical and chemical properties [1–4]. Perovskite oxides are particularly important as ferroelectrics in numerous applications ranging from medical ultrasound to sonar [5–7]. The large diversity of perovskites oxides could be further increased by anion substitution. For example, the photovoltaic performance can be boosted through halide anions substitution for oxygen in oxide perovskites [8]. As another example, nitrogen substitution for oxygen enriches the possible perovskite structures and their properties due to the concomitant interaction between oxygen and nitrogen ions [9]. The investigation of perovskite oxynitrides (ABO_2N) has rapidly become a highly important subject area because they represent an emerging class of materials offering the prospect of optimized properties and potential applications in many field, such as visible-light photocatalysts for water splitting, nontoxic pigments, and colossal magnetoresistance [10–20]. The different ionicities/covalencies between O and N ions may also induce the formation of strong polar perovskite structures, which hold the potential for piezoelectric and ferroelectric applications. In 2007, Caracas and Cohen predicted the polar ordered oxynitride perovskite $YSiO_2N$ with high predicted spontaneous polarization and large nonlinear optic coefficient [21].This phase was synthesized in a diamond anvil cell from YN and SiO_2 in 2017 [22].

Much oxynitride synthesis is done by ammonization of oxides, which results in random substitution of O by N, resulting in nonpolar structure [10,17,23]. Finding suitable starting materials for solid state synthesis is a challenge, as N bonds are either very strong or very unstable. For decades, pressure has been widely used as a powerful tool in the discovery of materials inaccessible at ambient conditions. Thus $YSiO_2N$ was synthesized in a polar perovskite phase under high-temperature and high-pressure conditions [22].

Despite the possibility for many novel phases with enhanced functionality, there are very limited studies on the exploration of pressure-induced polar structures in oxynitrides, leaving the rationally design of the synthesizable polar oxynitride perovskites unsettled. To tackle this problem, it is crucial to understand the thermodynamically stable structures and their properties, which has become possible becasue of the development of crystal structure prediction methods. In this work, we first predicted the high-pressure phase diagrams of various oxynitride systems using swarm-intelligence-based structure prediction methods [24–26]. The predictions reveal several pressure-induced polar oxynitrides. Further calculations indicate that the long-thought ferroelectric phase of oxynitrides can be stable and synthesized under epitaxial strain conditions.

Global structural optimization was performed using the CALYPSO code [24–26] with the particle swarm optimization algorithm, which has successfully predicted structures of various systems [27–32]. The energetic calculations were carried out in the framework of density functional theory (DFT) within the Perdew-Burke-Ernzerhof revised for solids (PBEsol) [33] functional, as implemented in the Vienna *ab initio* simulation package (VASP) code [34]. The previous

---

[*] Current address: Department of Physics, Rutgers University, Newark, NJ 07102, USA; li.zhu@rutgers.edu

[†] rcohen@carnegiescience.edu

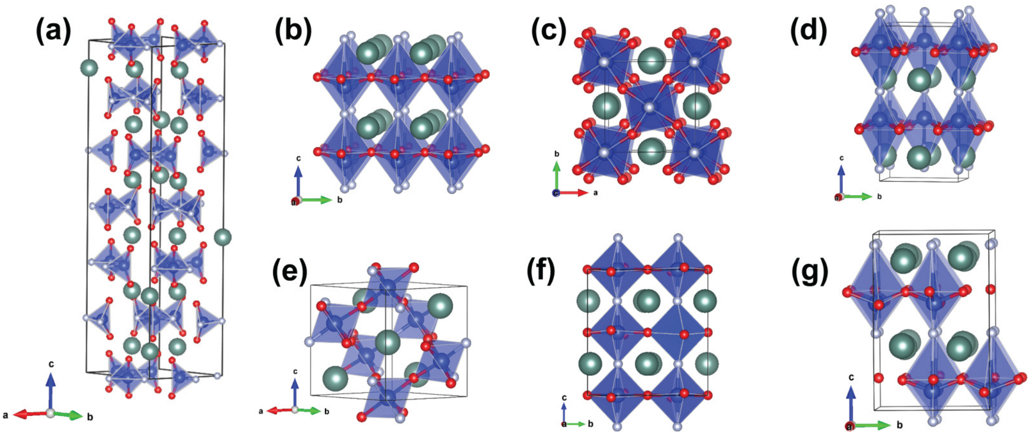

FIG. 1. Crystal structures of oxynitride compounds in (a) the $P6_122$ structure, (b) the $P4mm$ structure, (c) the $I4/mcm$ structure, (d) the $I4cm$ structure, (e) the $P3_121$ structure, (f) the $P3_2$ structure, and (g) the $Cmc2_1$ structure. Cyan, blue, red, and light grey spheres represent Y/La/Bi, Si/Ge/Hf, O, and N atoms, respectively.

study verified that the PBEsol functional can reproduce the experimental results very well compared to the other functionals [35]. The all-electron projector augmented wave (PAW) method [36] as adopted with the pseudopotentials taken from the VASP library where $4s^24p^64d^15s^2$, $5s^25p^65d^16s^2$, $5d^{10}6s^26p^3$, $3s^23p^2$, $4s^24p^2$, $5d^26s^2$, $2s^22p^4$, and $2s^22p^5$ were treated as valence electrons for Y, La, Bi, Si, Ge, Hf, O, and N, respectively. The electronic wave functions were expanded in a plane-wave basis set with a cutoff energy of 520 eV. Monkhorst-Pack k-point meshes [37] with a grid of spacing $0.04 \times 2\pi$ Å^{-1} for Brillouin zone sampling were chosen after checking for convergence. For example, we used a $8 \times 8 \times 6$ k point for the five-atom perovskite structures. To determine the dynamical stability of the studied structures, we performed phonon calculations by using the finite displacement approach, as implemented in the PHONOPY code [38].

Structure prediction calculations were performed at a pressure of 30 GPa with up to four formula units (f.u.) per simulation cell. We uncovered a group of new structures for the oxynitrides at 30 GPa. We take the crystal phases identified by the structure search process and compute their enthalpies to determine the most stable structure for each composition. The enthalpies were calculated by optimizing the cell parameters and the atomic positions at each pressure using the conjugate gradient algorithm implemented in the VASP code [34]. The enthalpy curves (Fig. 2) show the relative thermodynamic stabilities of the predicted structures. The hexagonal $P6_122$ structure (Fig. 1(a), see Ref. [39]) is most stable at ambient pressure for all of these compounds. Under pressure, however, we find many new oxynitride phases.

At 30 GPa, the most stable structures for $LaSiO_2N$, $LaGeO_2N$, and $BiSiO_2N$ are predicted to be tetrahedrally coordinated trigonal polar phases [Figs. 2(d)–2(f)]. These structures are piezoelectric, but cannot be ferroelectric by symmetry. Nonpolar, centrosymmetric, perovskite phases are favorable above ∼18 GPa and ∼7 GPa for $YSiO_2N$ ($I4/mcm$) and $BiSiO_2N$ ($Cmcm$), respectively. $YGeO_2N$ and $YHfO_2N$ are more stable in nonperovskite structures at high pressures. The structural parameters for these structures are in the supplemental material [40]. We have computed the phonon dispersion for all of these structures, and find that these compounds are dynamically stable (Fig. S1). We noticed that a previous study predicted a variety of dynamically stable oxynitride structures including polar $Pmm2$ and nonpolar $P4/mmm$ phases [18], which also can be found from our structure prediction results. However, these are relatively high-enthalpy phases compared with our predicted structures (Fig. 2).

We find that the $P4mm$ structure of $BiSiO_2N$ is very close in enthalpy to the most stable structure under pressure. Perovskite phase stability is often governed by the radius ratio of the A and B cations [41]. Indeed, we find that the larger value of r_A/r_B, the more stable the $P4mm$ phase, where r_A and r_B are the ionic radii [42] of atoms at A and B sites, respectively [Fig. 3(a)]. Within $P4mm$ symmetry, $BiSiO_2N$ is relatively more stable than other compositions considered here, but imaginary phonon frequencies show that it is dynamically unstable. $LaSiO_2N$ is another low enthalpy $P4mm$ structure; it is only 90 meV / f.u. higher in enthalpy than the $P3_121$ structure at 30 GPa.

The $P4mm$ ferroelectric phase of $YSiO_2N$ was calculated to be metastable with the local density approximation [43,44] and Troullier-Martins pseudopotentials [45] in a previous study [21]. However, we find that the $P4mm$ structure of $YSiO_2N$ is dynamically unstable with the PBEsol functional [33] in the current study, although we were able to reproduce the earlier results using the same pseudopotentials as were used in Ref. [21]. In spite of its apparent instability according to DFT, synthesis of the $P4mm$ structure of $YSiO_2N$ was reported under high pressure and temperature conditions [22]. How can one explain its apparent stability? We found that the $I4cm$ structure of $YSiO_2N$ [Fig. 1(d)] is slightly lower in energy than the $P4mm$ structure [Fig. 2(a)], and is dynamically stable (Fig. S4). The $I4cm$ $YSiO_2N$ shares nearly the same XRD patterns with the $P4mm$ phase (Fig. S5). We performed first-principles molecular dynamics for $4\sqrt{2} \times 4\sqrt{2} \times 4$ (160 atoms) supercells for temperatures from 300–600 K starting from the $I4cm$ structure, and found it stable up to 600 K under compressive epitaxial strain and to 400 K under no or extensional strain. There is a possibility that the $I4cm$ structure of $YSiO_2N$ was actually synthesized rather than the $P4mm$ structure. However, our enthalpy calculations suggest that the $I4cm$ $YSiO_2N$ is unstable under high

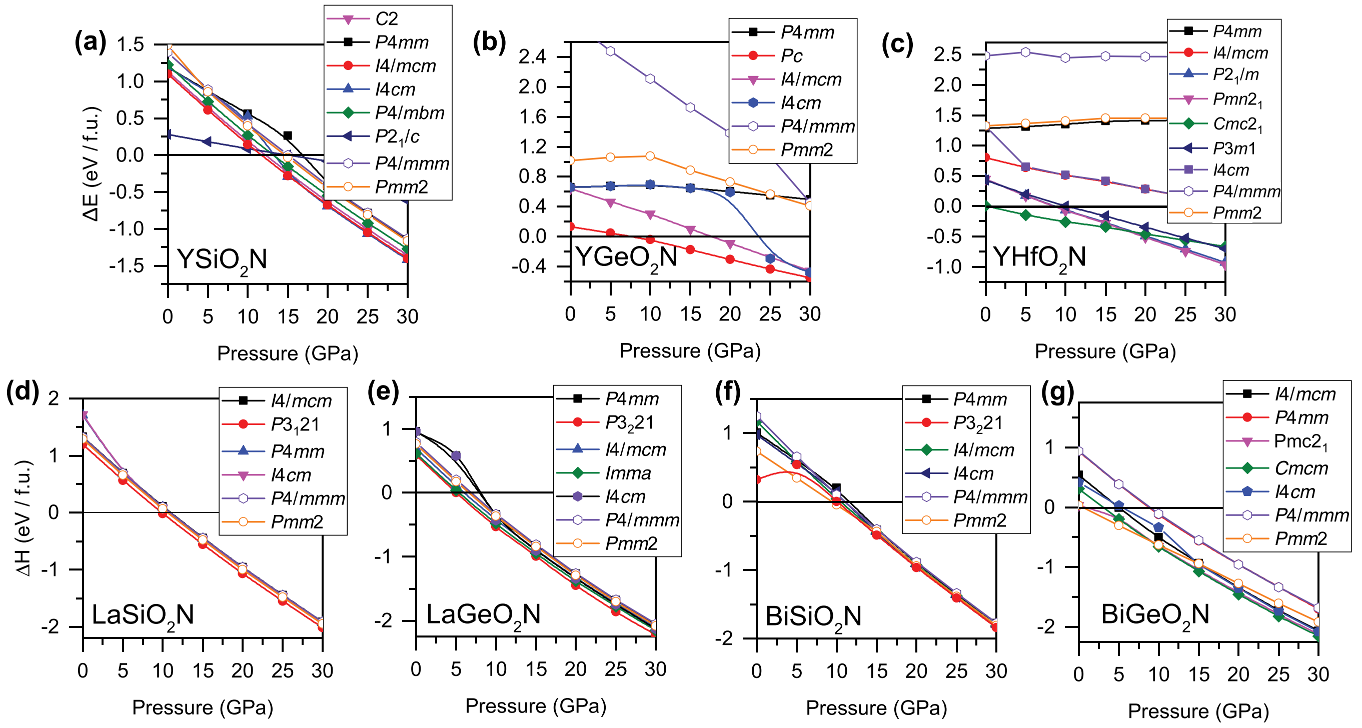

FIG. 2. Calculated enthalpies per formula unit (f.u.) of various predicted structures as functions of pressure with respect to the $P6_122$ structure of the oxynitrides.

pressures. At the pressures above 10 GPa, the *I*4*cm* structure transforms into the most stable *I*4/*mcm* structure after geometry optimization [Fig. 2(a)], suggesting that there is no energy barrier between these two phases. Thus *I*4*cm* might form on decompression of *I*4/*mcm* $YSiO_2N$ as pressure is decreased. So again, how can we explain the report of polar tetragonal perovskite $YSiO_2N$ observed *in situ* at high pressures [22]?

YN was used as one of the precursors in the experimental synthesis. YN adopts the rocksalt-type face-centered cubic structure, and the lattice of $YSiO_2N$ can share N atoms along the [110] directions on the YN surface (Fig. S6). The lattice mismatch between YN and $YSiO_2N$ induces around 2% epitaxial (extensional) strain, which could stabilize the *P*4*mm* structure of $YSiO_2N$. Previous studies have shown that epitaxial strain can stabilize ferroelectric structures or trigger spontaneous polarization in perovskite oxides [46–49]. To investigate the effect of applied epitaxial strain on the stability of perovskite oxynitrides, we fix the lattice parameters of *a* and *b* with −5% to 5% strains, and relax *c* axis and atomic positions. We next calculate the phonon dispersion of these strained structures, which reveal that the extensional strain hardens the phonon modes. Thus we propose that the successful synthesis of the *P*4*mm* structure of $YSiO_2N$ can be ascribed to epitaxial strain on YN.

Nonhydrostatic pressure has previously been found to promote formation of metastable materials. For example, a large uniaxial stress was found to promote the synthesis of the cubane-derived nanothreads in the diamond anvil cell [50]. Since nonhydrostatic pressure or epitaxial strain might promote formation of ferroelectric oxynitrides, we studied our candidates polar oxynitrides under epitaxial strain (nonhydrostatic pressure) as well as hydrostatic pressure.

The softest phonon modes for the *P*4*mm* structures of the oxynitrides as a function of epitaxial strain indicates which compounds and conditions are at least metastable (Fig. 4). We find that the *P*4*mm* perovskite structures of $YGeO_2N$, $LaSiO_2N$, and $LaGeO_2N$ are metastable at zero applied stress (Fig. S7), and the phonon modes harden with the increasing stress. The electric band gaps were calculated using the modified Becke-Johnson exchange potential in combination with L(S)DA correlation, which yields more accurate band gaps for semiconductors [51,52]. Our calculations suggest that the studied oxynitrides are insulators with large bandgaps, 4.3 eV in the *P*4*mm* $YSiO_2N$, 4.1 eV in the *I*4*cm* $YSiO_2N$, 3.1 eV in the *P*4*mm* $YGeO_2N$, 2.7 eV in the *P*4*mm* $LaSiO_2N$, and 2.8 eV in the *P*4*mm* $LaGeO_2N$. The computed polarizations of $2.21\ C/m^2$ ($YGeO_2N$), $1.27\ C/m^2$ ($LaSiO_2N$), and $0.97\ C/m^2$ ($LaGeO_2N$) are much larger than that of $BaTiO_3$, and the values of the polarization are among the highest ever reported so far in the literature.

The dynamical stability of these ferroelectric phases makes it likely they can be synthesized at ambient pressure using layer-by-layer growth methods such as pulzed laser deposition (PLD) [53], molecular beam epitaxy (MBE) [54] or chemical vapor deposition (CVD) etc., which have been used to synthesize many metastable materials, including diamond and carbon nanotubes [55,56]. For $LaGeO_2N$, the structure collapsed when the epitaxial strain reaches 5%, resulting in the imaginary phonon frequencies again. The *P*4*mm* phases of $BiSiO_2N$ and $BiGeO_2N$ remain dynamically unstable at the epitaxial strain of -5% to 5%. A trend of the modes with the strain for $YHfO_2N$ is opposite to the others, the blue curve in Fig. 4. The compressive strain by -5% stabilizes the *P*4*mm* structure of $YHfO_2N$.

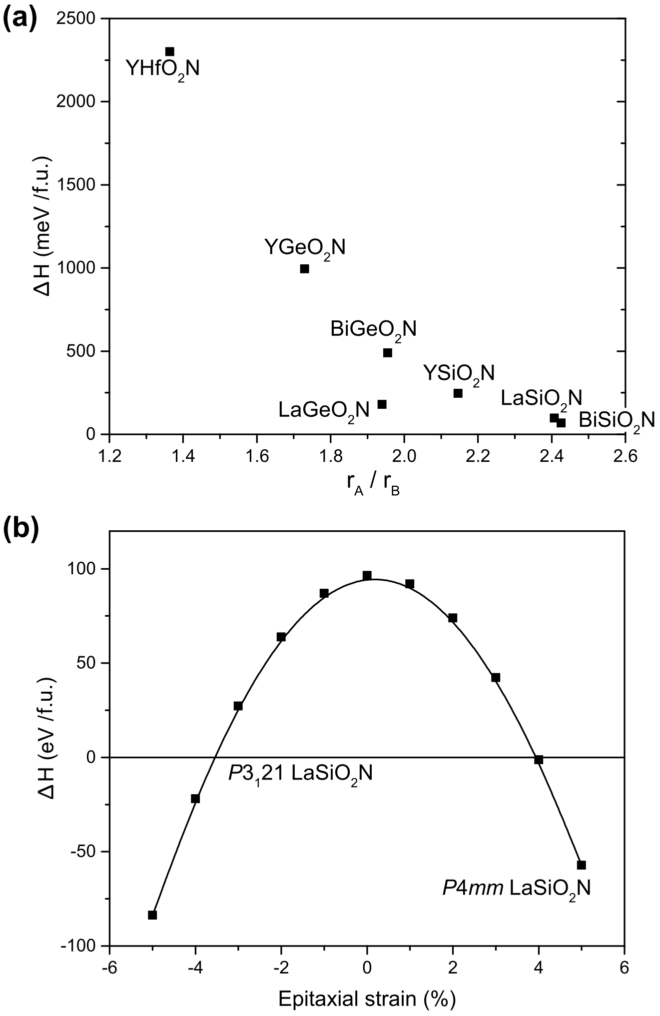

FIG. 3. (a) The calculated enthalpies of the $P4mm$ structure with respect to the most stable structure of the various oxynitrides at 30 GPa. (b) The calculated enthalpies of the $P4mm$ structure of $LaSiO_2N$ as a function of epitaxial strain with respect to the $P3_121$ structure at 30 GPa. Positive strains here and elsewhere in this paper are extensional.

However, we find other compositions which may be more stable and promising for further study. From the enthalpy perspective, $P4mm$ $LaSiO_2N$ is promising for synthesis under extensional epitaxial strain at 30 GPa [Fig. 3(b)]. The dynamic stabilities of the $P4mm$ $LaSiO_2N$ were examined by calculating the phonon spectra, and no imaginary phonon frequencies were found in the whole Brillouin zone under epitaxial strain of −5%, −4%, and 4% at 30 GPa (Fig. S3). The stability of the strained $P4mm$ $LaSiO_2N$ is encouraging for future synthesis efforts. Besides the $P4mm$ $LaSiO_2N$, we found the ferroelectric $Cmc2_1$ structures of $BiSiO_2N$ and $BiGeO_2N$ are also metastable at ambient pressure (Fig. S8), which are also very promising for further experimental studies.

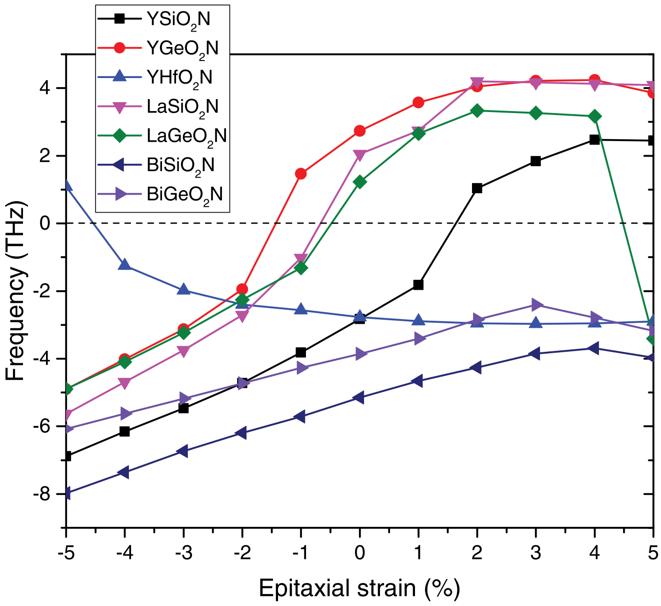

FIG. 4. Soft phonon modes for the $P4mm$ structures of the oxynitrides as functions of the epitaxial strain at ambient pressure.

In summary, we have combined automatic structure searching methods with first-principles calculations to investigate the phase stability of oxynitrides. Our study reveals that the dynamical stability of the ferroelectric phase of oxynitrides is sensitive to the epitaxial strain. The energy calculations suggest that it is promising to synthesize ferroelectric oxynitrides at ambient pressure using nonequilibrium synthesis methods or under high pressure and epitaxial strain. This work also provides a vision for searching synthesizable ferroelectric oxynitrides by controlling the size ratio of different elements at the A/B site of perovskite structures.

This work is supported by U. S. Office of Naval Research Grants No. N00014-17-1-2768 and N00014-20-1-2699, and the Carnegie Institution for Science. Computations were supported by DOD HPC, Carnegie computational resources, and REC gratefully acknowledges the Gauss Centre for Supercomputing e.V. for funding this project by providing computing time on the GCS Supercomputer SuperMUC-NG at Leibniz Supercomputing Centre (LRZ).

---

[1] T. Okuda, K. Nakanishi, S. Miyasaka, and Y. Tokura, Large thermoelectric response of metallic perovskites: $Sr_{1-x}La_xTiO_3$ ($0 <\sim x <\sim 0.1$), Phys. Rev. B **63**, 113104 (2001).

[2] G. Sághi-Szabó, R. E. Cohen, and H. Krakauer, First-Principles Study of Piezoelectricity in $PbTiO_3$, Phys. Rev. Lett. **80**, 4321 (1998).

[3] Z. Kutnjak, J. Petzelt, and R. Blinc, The giant electromechanical response in ferroelectric relaxors as a critical phenomenon, Nature (London) **441**, 956 (2006).

[4] M. K. Wu, J. R. Ashburn, C. J. Torng, P. H. Hor, R. L. Meng, L. Gao, Z. J. Huang, Y. Q. Wang, and C. W. Chu, Superconductivity at 93 K in a New Mixed-Phase Y-Ba-Cu-O

Compound System at Ambient Pressure, Phys. Rev. Lett. **58**, 908 (1987).

[5] G. H. Haertling, Ferroelectric ceramics: History and technology, J. Am. Ceram. Soc. **82**, 797 (1999).

[6] B. W. Wessels, Ferroelectric epitaxial thin films for integrated optics, Annu. Rev. Mater. Res. **37**, 659 (2007).

[7] J. F. Scott, Applications of modern ferroelectrics, Science **315**, 954 (2007).

[8] A. K. Jena, A. Kulkarni, and T. Miyasaka, Halide perovskite photovoltaics: Background, status, and future prospects, Chem. Rev. **119**, 3036 (2019).

[9] A. Fuertes, Chemistry and applications of oxynitride perovskites, J. Mater. Chem. **22**, 3293 (2012).

[10] Y.-I. Kim, P. M. Woodward, K. Z. Baba-Kishi, and C. W. Tai, Characterization of the structural, optical, and dielectric properties of oxynitride perovskites AMO_2N (A = Ba, Sr, Ca; M = Ta, Nb), Chem. Mater. **16**, 1267 (2004).

[11] R. L. Withers, Y. Liu, P. Woodward, and Y.-I. Kim, Structurally frustrated polar nanoregions in $BaTaO_2N$ and the relationship between its high dielectric permittivity and that of $BaTiO_3$, Appl. Phys. Lett. **92**, 102907 (2008).

[12] Y. Hinuma, H. Moriwake, Y.-R. Zhang, T. Motohashi, S. Kikkawa, and I. Tanaka, First-principles study on relaxor-type ferroelectric behavior without chemical inhomogeneity in $BaTaO_2N$ and $SrTaO_2N$, Chem. Mater. **24**, 4343 (2012).

[13] T. Yajima, F. Takeiri, K. Aidzu, H. Akamatsu, K. Fujita, W. Yoshimune, M. Ohkura, S. Lei, V. Gopalan, K. Tanaka, C. M. Brown, M. A. Green, T. Yamamoto, Y. Kobayashi, and H. Kageyama, A labile hydride strategy for the synthesis of heavily nitridized $BaTiO_3$, Nat. Chem. **7**, 1017 (2015).

[14] C. Le Paven-Thivet, A. Ishikawa, A. Ziani, L. Le Gendre, M. Yoshida, J. Kubota, F. Tessier, and K. Domen, Photoelectrochemical properties of crystalline perovskite lanthanum titanium oxynitride films under visible light, J. Phys. Chem. C **113**, 6156 (2009).

[15] M. Higashi, K. Domen, and R. Abe, Fabrication of an efficient $BaTaO_2N$ photoanode harvesting a wide range of visible light for water splitting, J. Am. Chem. Soc. **135**, 10238 (2013).

[16] S. Balaz, S. H. Porter, P. M. Woodward, and L. J. Brillson, Electronic structure of tantalum oxynitride perovskite photocatalysts, Chem. Mater. **25**, 3337 (2013).

[17] M. Jansen and H. P. Letschert, Inorganic yellow-red pigments without toxic metals, Nature (London) **404**, 980 (2000).

[18] C. Kim, G. Pilania, and R. Ramprasad, Machine learning assisted predictions of intrinsic dielectric breakdown strength of ABX_3 perovskites, J. Phys. Chem. C **120**, 14575 (2016).

[19] W. Li, E. Ionescu, R. Riedel, and A. Gurlo, Can we predict the formability of perovskite oxynitrides from tolerance and octahedral factors? J. Mater. Chem. A **1**, 12239 (2013).

[20] H.-C. Wang, J. Schmidt, S. Botti, and M. A. L. Marques, A high-throughput study of oxynitride, oxyfluoride and nitrofluoride perovskites, J. Mater. Chem. A **9**, 8501 (2021).

[21] R. Caracas and R. E. Cohen, Prediction of polar ordered oxynitride perovskites, Appl. Phys. Lett. **91**, 092902 (2007).

[22] R. Vadapoo, M. Ahart, M. Somayazulu, N. Holtgrewe, Y. Meng, Z. Konopkova, R. J. Hemley, and R. E. Cohen, Synthesis of a polar ordered oxynitride perovskite, Phys. Rev. B **95**, 214120 (2017).

[23] P. E. Morgan and P. J. Carroll, The crystal structures of $CeSiO_2N$ and $LaSiO_2N$, J. Mater. Sci. **12**, 2343 (1977).

[24] Y. Wang, J. Lv, L. Zhu, and Y. Ma, Crystal structure prediction via particle-swarm optimization, Phys. Rev. B **82**, 094116 (2010).

[25] Y. Wang, J. Lv, L. Zhu, and Y. Ma, CALYPSO: A method for crystal structure prediction, Comput. Phys. Commun. **183**, 2063 (2012).

[26] B. Gao, P. Gao, S. Lu, J. Lv, Y. Wang, and Y. Ma, Interface structure prediction via calypso method, Sci. Bull. **64**, 301 (2019).

[27] L. Zhu, H. Wang, Y. Wang, J. Lv, Y. Ma, Q. Cui, Y. Ma, and G. Zou, Substitutional Alloy of Bi and Te at High Pressure, Phys. Rev. Lett. **106**, 145501 (2011).

[28] L. Zhu, Z. Wang, Y. Wang, G. Zou, H.-k. Mao, and Y. Ma, Spiral chain O_4 form of dense oxygen, Proc. Natl. Acad. Sci. USA **109**, 751 (2012).

[29] L. Zhu, H. Liu, C. J. Pickard, G. Zou, and Y. Ma, Reactions of xenon with iron and nickel are predicted in the Earth's inner core, Nat. Chem. **6**, 644 (2014).

[30] Y. Wang, J. Lv, L. Zhu, S. Lu, K. Yin, Q. Li, H. Wang, L. Zhang, and Y. Ma, Materials discovery via CALYPSO methodology, J. Phys.: Condens. Matter **27**, 203203 (2015).

[31] L. Zhu, G. M. Borstad, R. E. Cohen, and T. A. Strobel, Pressure-induced polymorphism in SrB_6 and deformation mechanisms of covalent networks, Phys. Rev. B **100**, 214102 (2019).

[32] L. Zhu, G. M. Borstad, H. Liu, P. A. Guńka, M. Guerette, J.-A. Dolyniuk, Y. Meng, E. Greenberg, V. B. Prakapenka, B. L. Chaloux, A. Epshteyn, R. E. Cohen, and T. A. Strobel, Carbon-boron clathrates as a new class of sp^3-bonded framework materials, Sci. Adv. **6**, eaay8361 (2020).

[33] J. P. Perdew, A. Ruzsinszky, G. I. Csonka, O. A. Vydrov, G. E. Scuseria, L. A. Constantin, X. Zhou, and K. Burke, Restoring the Density-Gradient Expansion for Exchange in Solids and Surfaces, Phys. Rev. Lett. **100**, 136406 (2008).

[34] G. Kresse and J. Furthmüller, Efficient iterative schemes for ab initio total-energy calculations using a plane-wave basis set, Phys. Rev. B **54**, 11169 (1996).

[35] L. He, F. Liu, G. Hautier, M. J. T. Oliveira, M. A. L. Marques, F. D. Vila, J. J. Rehr, G.-M. Rignanese, and A. Zhou, Accuracy of generalized gradient approximation functionals for density-functional perturbation theory calculations, Phys. Rev. B **89**, 064305 (2014).

[36] P. E. Blöchl, Projector augmented-wave method, Phys. Rev. B **50**, 17953 (1994).

[37] H. J. Monkhorst and J. D. Pack, Special points for Brillouin-zone integrations, Phys. Rev. B **13**, 5188 (1976).

[38] A. Togo and I. Tanaka, First principles phonon calculations in materials science, Scr. Mater. **108**, 1 (2015).

[39] L. Ouyang, H. Yao, S. Richey, Y.-N. Xu, and W. Y. Ching, Crystal structure and properties of $YSiO_2N$, Phys. Rev. B **69**, 094112 (2004).

[40] See Supplemental Material at http://link.aps.org/supplemental/10.1103/PhysRevMaterials.5.114404 for the structural parameters and additional calculation details.

[41] V. M. Goldschmidt, Die gesetze der krystallochemie, Naturwissenschaften **14**, 477 (1926).

[42] R. D. Shannon and C. T. Prewitt, Effective ionic radii in oxides and fluorides, Acta Crystallogr. Sect. B **25**, 925 (1969).

[43] P. Hohenberg and W. Kohn, Inhomogeneous electron gas, Phys. Rev. **136**, B864 (1964).

[44] D. M. Ceperley and B. J. Alder, Ground State of the Electron Gas by a Stochastic Method, Phys. Rev. Lett. **45**, 566 (1980).

[45] N. Troullier and J. L. Martins, Efficient pseudopotentials for plane-wave calculations, Phys. Rev. B **43**, 1993 (1991).

[46] J. H. Haeni, P. Irvin, W. Chang, R. Uecker, P. Reiche, Y. L. Li, S. Choudhury, W. Tian, M. E. Hawley, B. Craigo, A. K. Tagantsev, X. Q. Pan, S. K. Streiffer, L. Q. Chen, S. W. Kirchoefer, J. Levy, and D. G. Schlom, Room-temperature ferroelectricity in strained $SrTiO_3$, Nature (London) **430**, 758 (2004).

[47] K. J. Choi, Enhancement of Ferroelectricity in strained $BaTiO_3$ thin films, Science **306**, 1005 (2004).

[48] S. Liu, Y. Kim, L. Z. Tan, and A. M. Rappe, Strain-Induced Ferroelectric Topological Insulator, Nano Lett. **16**, 1663 (2016).

[49] R. Xu, J. Huang, E. S. Barnard, S. S. Hong, P. Singh, E. K. Wong, T. Jansen, V. Harbola, J. Xiao, B. Y. Wang, S. Crossley, D. Lu, S. Liu, and H. Y. Hwang, Strain-induced room-temperature ferroelectricity in $SrTiO_3$ membranes, Nat. Commun. **11**, 3141 (2020).

[50] H.-T. Huang, L. Zhu, M. D. Ward, T. Wang, B. Chen, B. L. Chaloux, Q. Wang, A. Biswas, J. L. Gray, B. Kuei, G. D. Cody, A. Epshteyn, V. H. Crespi, J. V. Badding, and T. A. Strobel, Nanoarchitecture through strained molecules: Cubane-derived scaffolds and the smallest carbon nanothreads, J. Am. Chem. Soc. **142**, 17944 (2020).

[51] A. D. Becke and E. R. Johnson, A simple effective potential for exchange, J. Chem. Phys. **124**, 221101 (2006).

[52] F. Tran and P. Blaha, Accurate Band Gaps of Semiconductors and Insulators with a Semilocal Exchange-Correlation Potential, Phys. Rev. Lett. **102**, 226401 (2009).

[53] H. M. Smith and A. Turner, Vacuum deposited thin films using a ruby laser, Appl. Opt. **4**, 147 (1965).

[54] A. Y. Cho and J. Arthur, Molecular beam epitaxy, Prog. Solid State Chem. **10**, 157 (1975).

[55] Y.-f. Meng, C.-s. Yan, J. Lai, S. Krasnicki, H. Shu, T. Yu, Q. Liang, H.-k. Mao, and R. J. Hemley, Enhanced optical properties of chemical vapor deposited single crystal diamond by low-pressure/high-temperature annealing, Proc. Natl. Acad. Sci. USA **105**, 17620 (2008).

[56] A. M. Cassell, J. A. Raymakers, J. Kong, and H. Dai, Large scale CVD synthesis of single-walled carbon nanotubes, J. Phys. Chem. B **103**, 6484 (1999).